Catalysis Today 213 (2013) 135–144

Contents lists available at SciVerse ScienceDirect

Catalysis Today

journal homepage: www.elsevier.com/locate/cattod

Comparison of $Ru/La_2O_2CO_3$ performance in two different membrane reactors for hydrogen production

Betina Faroldi, María Laura Bosko, John Múnera, Eduardo Lombardo, Laura Cornaglia*

Instituto de Investigaciones en Catálisis y Petroquímica – INCAPE (FIQ, UNL-CONICET), Santiago del Estero, 2829-3000 Santa Fe, Argentina

ARTICLE INFO

Article history:
Received 30 November 2012
Received in revised form 8 February 2013
Accepted 11 February 2013
Available online 17 April 2013

Keywords:
Methane combined reforming
Ruthenium
$La_2O_2CO_3$
Hydrogen production
Membrane reactor

ABSTRACT

Ruthenium catalysts supported on a lanthanum oxycarbonate phase ($La_2O_2CO_3$) with high surface area were prepared. All solids were stable for at least 90 h on stream in the combined dry reforming and oxidation of methane reactions. The catalyst with more stable metallic Ru species was selected to be studied under the more severe conditions of membrane reactors. A double tubular membrane reactor was built using a commercial self-standing membrane or a composite Pd/NaAPSS membrane. The Pd membrane reactor exhibited a higher H_2 permeated/CH_4 fed ratio at 450 °C that could be related to its higher hydrogen permeability. The comparison of the catalytic behavior of Ru catalysts supported on high surface area lanthanum oxycarbonate and La_2O_3–SiO_2 binary support in a membrane reactor was performed at 550 °C. On the retentate side, the molar composition of CO_2 was similar to that of CH_4 when the $Ru/La_2O_2CO_3$ catalyst was employed, which suggests that this solid did not favor the RWGS reaction under DRM conditions producing a higher H_2 permeated/CH_4 fed ratio. The Ru catalysts showed a similar performance to that of our best Rh solids when the fractions of the reaction equilibration and H_2 permeated/(CH_4 fed × permeation area) ratio were compared.

1. Introduction

When the goal of the methane reforming reactions is to produce hydrogen for use in a fuel cell, they can be carried out in membrane reactors that combine reaction and hydrogen separation process in a single device. The highly endothermic dry reforming of methane can be coupled with an exothermic reaction such as the partial oxidation of methane. By combining both reactions, the H_2/CO ratios could evolve to increase the practical interest of this process in conventional fixed-bed reactors. In addition, membrane reactors allow improving the performance with respect to hydrogen in this system limited by thermodynamic equilibrium.

Different types of membranes have been recently applied in membrane reactors for the dry reforming of methane reaction [1–3]. In most cases, an increase in methane conversion is observed when H_2 is extracted from the reaction system. The results are highly dependent on the conditions under which the reactions are carried out, such as space velocity (W/F), dilution of the CO_2/CH_4 mixture, membrane selectivity and permeation capacity, deposition of carbon from the catalysts, temperature and reactor pressure. However, few experimental studies using methane reforming and partial oxidation reactions coupled in a membrane reactor have been reported in the literature [4,5].

In a recent paper, Oyama et al. [3] studied the methane dry-reforming and steam reforming reactions as a function of pressure (1–20 atm) in a membrane reactor. They found that at high pressures the yield of hydrogen in the dry-reforming reaction levels off because part of the hydrogen reacts with CO_2 through the reverse water-gas shift reaction.

Many Pd composite membranes have been fabricated on stainless steel supports [6]. Non-metallic materials, such as oxides [7] or zeolites [8,9], can be used as modifiers of support roughness and average pore size, and they are deposited between the support and the Pd alloy films. In previous studies, we employed a novel material, NaA zeolite, as support modifier [8,9] while the Pd selective layer was deposited by electroless plating.

In our group, we employed composite and self-supported commercial Pd/Ag membranes to produce ultrapure hydrogen. This commercial membrane was selected due to its stability and robustness [10,12] at temperatures as high as 550 °C, usually required by the endothermic methane reforming reactions. We also compared the behavior of different La-based noble metal catalysts in a membrane reactor for the carbon dioxide reforming of methane with and without oxygen addition [5,10–12]. The best performing formulations reported so far are Rh and Ru supported on a binary La_2O_3–SiO_2 support [5,11]. Both solids show high metal dispersion and the presence of an amorphous lanthanum disilicate confers an appropriate metal-support interaction.

* Corresponding author. Tel.: +54 342 4536861; fax: +54 342 4536861.
E-mail addresses: lmcornag@fiq.unl.edu.ar, lcornaglia2002@yahoo.com (L. Cornaglia).

0920-5861/$ – see front matter © 2013 Elsevier B.V. All rights reserved.
http://dx.doi.org/10.1016/j.cattod.2013.02.024

The aim of this work is to develop a catalyst with lower costs, high resistance to carbon deposition, and high hydrogen yield. Among noble metals, Ru is an interesting alternative because its cost is significantly lower compared to Rh.

Ruthenium catalysts [12] supported on commercial La_2O_3 have good activity and stability and very low carbon deposition for the methane dry reforming reaction. However, the dispersion of ruthenium on these solids presents very low values. A key role has been assigned to the lanthanum oxycarbonate phase in the stability of lanthanum-based catalysts. This phase reacts with the carbon deposited on the catalyst surface avoiding the solid deactivation.

In this study, we present a novel Ru catalyst supported on lanthanum oxycarbonate with high surface area for use in membrane reactors. Two types of Pd-based membranes were employed to build the reactor, a pure Pd composite membrane and a self-standing commercial Pd–Ag one. The performances of both reactors were studied at 450 °C. A comparison was performed among the best catalysts developed in our group for the combined dry reforming and oxidation of methane reactions at 550 °C.

2. Materials and methods

2.1. Catalyst preparation and characterization

A high surface area lanthanum oxycarbonate phase was synthesized as support for Ru catalysts. La_2O_3 (Aldrich) was heated at 650 °C during 6 h in pure O_2 flow (UAP 5.0) to obtain a pure La_2O_3 crystalline phase. Then, a treatment with a solution of acetic acid (50%, v/v) was performed, stirring and drying at 80 °C to evaporate the liquid [13]. After that, the solids were dried at the same temperature for 6 h in a rotary evaporator (MR), and during 12 h in a vacuum oven (MV). All the supports were calcined at 400 °C in flowing O_2. The metal was added using a solution of $RuCl_3{\cdot}3H_2O$ by wet impregnation (Ru1) or by metal incorporation during the support synthesis (Ru2). The nominal Ru loading was 0.6 wt.% for all the catalysts.

The XRD patterns of the calcined solids and supports were obtained with an XD-D1 Shimadzu instrument, using Cu-Kα radiation at 30 kV and 40 mA. The scan rate was 1.0°/min for values between $2\theta = 10°$ and 70°.

The Raman spectra were recorded using a LabRam spectrometer (Horiba-Jobin-Yvon) coupled to an Olympus confocal microscope (a 100× objective lens was used for simultaneous illumination and collection), equipped with a CCD detector cooled to about −73 °C using the Peltier effect. In situ LRS measurements were performed in a Linkam high temperature cell. The powder catalyst was loaded and the gas stream flowed through the solids.

The XPS measurements were carried out using a multitechnique system (SPECS) equipped with a dual Mg/Al X-ray source and a hemispherical PHOIBOS 150 analyzer operating in the fixed analyzer transmission (FAT) mode. The spectra were obtained with pass energy of 30 eV; an Mg-Kα X-ray source was operated at 200 W and 12 kV. The XPS analyses were performed on the supports and on the solids after treatment with H_2 or CO_2 at 400 °C, carried out in the reaction chamber of the spectrometer. The spectral regions corresponding to La 3d, C 1s, O 1s, Si 2s, Ru 3d and Ru 3p core levels were recorded for each sample.

2.2. Synthesis and characterization of the Pd/NaAPSS composite membrane

Porous stainless steel (PSS) tubes (Mott Corporation, 316 L, 6.4 mm i.d., 9.5 mm o.d.). 0.1 μm grade were used as supports of the Pd membrane. Before deposition, one end of the PSS tube was welded to a non-porous stainless steel tube and the other one to a non-porous SS plug. The supports were cleaned in an alkaline solution [14] and dried overnight at 120 °C. After that, they were oxidized in stagnant air at 500 °C for 12 h. After oxidation, the surface of the porous metal supports was modified with NaA zeolite, employing hydrothermal synthesis with secondary growth. In order to prepare the synthesis gel, two precursors (alumina and silica) were mixed with vigorous stirring at the synthesis temperature (80 °C). The seeded support was placed vertically in a container with the synthesis gel for 6 h, and vacuum was applied. The inner and outer parts of the support were washed with deionized water, and then dried at 80 °C overnight [8]. One hydrothermal synthesis was performed.

The NaA zeolite modified substrates were activated by the conventional two-step $SnCl_2/PdCl_2$ procedure [9,15]. This sequence was repeated between three and six times to obtain the activation layer. Electroless plating (ELP) was used to coat the PSS with a continuous metallic layer. When the membrane was impermeable to liquid, the plating was carried out with vacuum in order to block the last remaining large pores. The activation-plating procedure was repeated until the composite membrane became impermeable to N_2 at room temperature and at a pressure difference of 10 kPa. More details about the NaA zeolite synthesis and the electroless plating are given elsewhere [9]. The film thickness was estimated from the weight gain after metal deposition and checked by SEM.

The H_2 permeation through the Pd membranes was measured using a membrane reactor in a temperature range of 400–550 °C and a trans-membrane pressure of 20 kPa.

The membrane reactor filled with quartz wool was heated in Ar flow to 400 °C, and then the feed was switched to pure hydrogen. Afterwards, the same procedure was carried out for the different temperatures under study.

2.3. Catalytic test

2.3.1. Conventional fixed-bed reactor

The catalyst (200 mg) was loaded into a tubular quartz reactor (inner diameter, 16 mm) which was placed in an electric oven. A thermocouple in a quartz sleeve was placed on top of the catalyst bed. The catalysts were heated up to 550 °C in Ar flow and then reduced in H_2 flow at the same temperature for 2 h. The catalytic tests were carried out at 550 °C with a $W/F = 2 \times 10^{-4}$ g h ml^{-1}.

2.3.2. Membrane reactor

The double tubular membrane reactor was built using a commercial self-standing membrane (dense Pd–Ag alloy, thickness = 75 μm, 3.1 mm o.d.), provided by REB Research and Consulting or a composite membrane synthesized by our group (Pd/NaAPSS, Pd layer thickness = 20 μm, 9.5 mm o.d.), with one end closed and an inner tube to allow the sweep gas flow (SG). The outer tube was made of commercial non-porous quartz (i.d. 9.5 and 16 mm for the commercial and composite membranes, respectively).

An inert sweep gas (Argon) was employed. To allow a better comparison, the sweep gas ratio was defined as the sweep gas flow rate/methane feed flow rate. The values were varied between 1.7 (10 ml min^{-1}) and 15.7 (90 ml min^{-1}) to study the effect of the sweep ratio [16].

Three reaction temperatures were employed (450, 500 and 550 °C) in the commercial membrane reactor. However, the Pd/NaAPSS membrane reactor was operated at 450 °C only, to avoid defect formation in the composite membrane. The catalyst (1.5 g), diluted with quartz chips (2.7 g), was packed in the outer annular region (shell side), leading to a permeation area of 7.5 and 7.9 cm^2 for the commercial and composite membranes, respectively. *In addition, part of the catalyst bed was placed 0.8 cm above the membrane to prevent its deterioration when exposed to the presence of O_2,*

Table 1
Surface area, Ru dispersion and XPS Ru/La ratios of Ru catalysts.

Solids	*D* [%][a]	Sg fresh [$m^2\ g^{-1}$]	Ru/La ratio[b] XPS
Ru2MR	18	35.2	0.005
Ru1MV	19	31.4	0.048
Ru2MV	14	33.4	0.008

[a] Dispersion calculated from CO chemisorption. The CO/Ru ratio was considered equal to 1.
[b] Ru 3p/La 3d intensity ratio calculated from XPS data.

leading to a reactor configuration formed by a fixed-bed reactor followed by a membrane reactor. More details are given elsewhere [5]. The inner side of the membrane in all runs was kept at atmospheric pressure.

After the reduction, the different mixtures were fed with a total reaction flow rate of 16.6 ml min^{-1} in both reactor types. For the dry reforming of methane, the [CH_4:CO_2:Ar] ratios were [1:1:1.2] and [1:1.9:0.3] and for the combined reforming of methane, with the addition of 10% O_2 partially or totally replacing Ar, the [CH_4:CO_2:O_2:Ar] ratios were [1:1:0.3:0.9] and [1:1.9:0.3:0].

The conversions were measured after a 1-h stabilization period. The reaction products and the permeated mixture for both reactor types were analyzed with two on-line thermal conductivity detector gas chromatographs: a Shimadzu GC-8A and a SRI 8610 C (SRI Instruments (USA)). The former instrument was equipped with a Porapak column, and the latter with a molecular sieve column. The carbon balance was close to one in all cases.

2.3.3. Thermodynamic calculations

The UniSim Design software package was used for simulation purposes of a Gibbs reactor. The Peng–Robinson equations of state were used to calculate the stream properties. To calculate the data, we employed the same total flow used in laboratory experiments. Even the dimensions given to the Gibbs reactor were equal to those used in the laboratory.

3. Results and discussion

3.1. Catalytic behavior and characterization of Ru/$La_2O_2CO_3$ in a conventional fixed-bed reactor for the dry and combined reforming of methane

Table 1 shows the metal dispersion, surface area and surface Ru/La ratios for Ru supported on lanthanum oxycarbonates.

From pure La_2O_3 (surface area equal to 5 $m^2\ g^{-1}$) and performing a treatment with acetic acid, it was possible to increase the surface area of the supports. When the solid was dried in a rotary evaporator (MR), a value of 15.1 $m^2\ g^{-1}$ was reached, whereas when using a vacuum oven (MV) the surface was 26.5 $m^2\ g^{-1}$.The surface area increased further after the incorporation of ruthenium, reaching values between 30 and 35 $m^2\ g^{-1}$ (Table 1). The metal dispersions for the three catalysts were between 14 and 19%. The presence of monoclinic $La_2O_2CO_3$-type Ia phase was observed by XRD and Laser Raman spectroscopy in all the catalysts (Fig. 1).

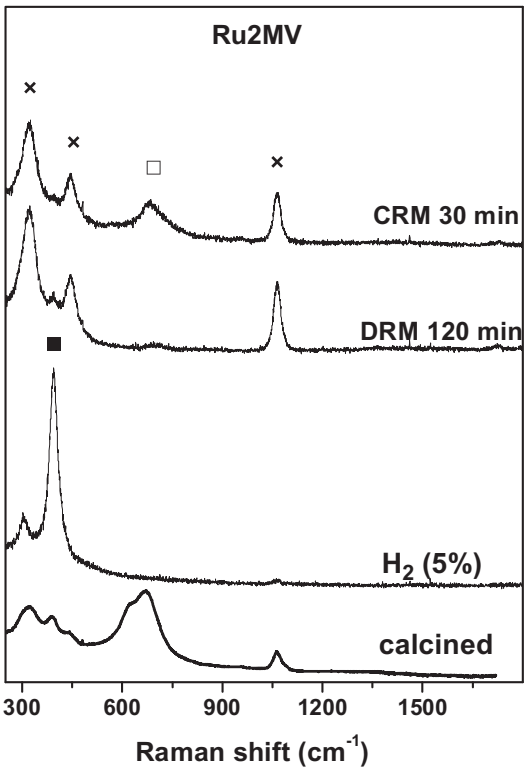

Fig. 1. In situ LRS of Ru2MV catalyst calcined, reduced and exposed at 550 °C to a reactant mixture with a composition of DRM (10% CH_4, 10% CO_2 and Ar) and CRM (CH_4/O_2 = 3). References: RuOx (□), La_2O_3 (■) and $La_2O_2CO_3$-type Ia (×).

The Ru/$La_2O_2CO_3$ catalytic activity for the dry and the combined reforming of methane (DRM and CRM) was measured. In the latter case, an increase in CH_4 conversion and H_2 production was achieved. These measurements were carried out with a 0.8 cm catalyst bed and high *W*/*F*. Under such conditions, the system reached thermodynamic equilibrium.

In the case of the addition of oxygen to the feed mixture, the reactions that might occur are the partial oxidation of methane (POM) and the dry reforming reaction (DRM) in addition to total oxidation of methane and the water gas shift reaction. Table 2 shows the measured methane and carbon dioxide conversions in comparison with equilibrium values calculated for both feed compositions, DRM and CRM.

To calculate the data, we employed the same total flow used in laboratory experiments. The dimensions given to the Gibbs reactor, applied for the thermodynamic equilibrium calculations were equal to those of the reactor used in the laboratory [11].

The methane conversion increased while the carbon dioxide conversion decreased when oxygen was added to the mixture, as expected, due to the occurrence of the total oxidation of methane. In the reactor outlet, oxygen was not chromatographically detected,

Table 2
Catalytic activity compared with theoretical equilibrium data for Ru/$La_2O_2CO_3$ catalysts at 550 °C.

CO_2:CH_4:O_2:Ar	Ru1MV		Ru2MV		Ru2MR		UniSim Design	
	X_{CH_4}	X_{CO_2}[a]	X_{CH_4}[a]	X_{CO_2}[a]	X_{CH_4}[a]	X_{CO_2}[a]	$X_{CH_{4\,eq}}$[b]	$X_{CO_{2\,eq}}$[b]
1:1:0:1.2	27.6	40.1	27.8	37.0	28.8	36.0	30.7	41.6
1:1:0.3:0.9	42.3	10.1	34.1	14.2	42.1	11.1	47.2	12.5
1.9:1:0:0.3	38.1	32.9	34.6	27.8	34.2	25.6	37.8	31.2
1.9:1:0.3:0	43.7	12.3	40.5	10.0	42.2	11.4	51.9	14.2

[a] Methane and carbon dioxide conversions, catalyst mass = 0.2 g, $W/F = 2 \times 10^{-4}$ g h ml^{-1}, reaction temperature = 550 °C.
[b] Calculated using UniSim Design software.

Table 3
Permeation features of the Pd based membranes.

Membrane	E (kJ mol)	P_0[a]	Pe[a] at 450 °C	K[b] at 450 °C	Ideal selectivity[c] (H_2/N_2) at 450 °C
Pd/NaAPSS	13.68	9.33×10^{-8}	9.6×10^{-9}	4.8×10^{-4}	2000
Pd–Ag commercial	24.64	2.61×10^{-7}	4.3×10^{-9}	5.7×10^{-5}	∞

[a] $mol\,s^{-1}\,m^{-1}\,Pa^{-0.5}$.
[b] $mol\,s^{-1}\,m^{-2}\,Pa^{-0.5}$ where

$$K_{H_2} = \frac{J}{[(P_{H_2,ret})^{0.5} - (P_{H_2,perm})^{0.5}]} \quad (3)$$

[c] Determined at 100 kPa.

indicating that it was completely consumed in the 0.8 cm catalyst bed.

As shown in Table 2, conversion values close to equilibrium were achieved in DRM conditions for all catalysts. However, in the case of CRM with CO_2/CH_4 ratio equal to 1.9, the methane conversion was always lower than the equilibrium value (42 ± 1.5 compared to 51.9%). This behavior could be due to the Ru re-oxidation that occurs when the metal is in contact with carbon dioxide rich atmospheres [17] which decrease the catalyst activity. A similar behavior has been previously observed for Ru/La_2O_3 solids [12,18].

In the case of CRM with CO_2/CH_4 ratio equal to 1.0, a different behavior was observed between the Ru2MV and Ru2MR catalysts. The Ru2MVsolid showed a methane conversion lower than the equilibrium value (34.1 compared to 47.2%). Note that Ru was incorporated during the support synthesis in both solids. In addition, all solids were stable for at least 90 h on stream and no carbon formation was observed by Laser Raman spectroscopy.

The reactivity of the lanthanum and ruthenium species was studied through in situ Raman measurements under different reaction atmospheres [19]. During the reduction treatment, the RuOx species were reduced to metallic ruthenium and the lanthanum oxycarbonate was decomposed to La_2O_3 and CO_2 (Fig. 1). The Ru1MV catalyst with the highest Ru/La ratio (Table 1) was the solid that presented greater reactivity of oxycarbonates to La_2O_3 (not shown) [19]. Under DRM and CRM conditions, the metallic Ru did not change its oxidation state for Ru1MV and Ru2MR catalysts. However, for the Ru2MV under CRM conditions, the Ru particles were partially re-oxidized and this might be the reason for the lower activity of this solid (Fig. 1).

When the lanthanum oxycarbonate decomposition was performed in an inert gas (Ar), a re-oxidation of the metallic Ru was observed in all catalysts [19]. For the Ru1MV solid, the RuOx species could be re-reduced under dry reforming of methane conditions. However, for the Ru2MR catalyst, the RuOx species could be re-reduced even in oxidizing atmospheres, such as the CRM mixture. From this evidence, the Ru2MR catalyst was selected for testing in membrane reactors [19] because this solid would be more stable at more severe conditions (high CO_2 content).

3.2. Membrane characterization

The permeation features of the palladium-based membranes are generally quantified in terms of permeability (Pe), permeance (K) or permeation flow (J). The flow of atomic hydrogen through the Pd membrane is the product of the diffusion coefficient and concentration gradient. The concentration of H atoms in the Pd layer may be related to the partial pressure of the gas, while the permeation flux (J, $mol\,s^{-1}\,m^{-2}$) is expressed by Sieverts' law:

$$J = \frac{Pe\left[(P_{H_2,ret})^{0.5} - (P_{H_2,perm})^{0.5}\right]}{l} \quad (1)$$

The value of $n = 0.5$, as an exponent of the permeate and retentate pressures $[(P_{H_2,ret})^{0.5} - (P_{H_2,perm})^{0.5}]$, would indicate that the rate determining step is the diffusion of H atoms through the metal film. For both membranes a linear correlation was observed between the permeation flux and the $[(P_{H_2,ret})^{0.5} - (P_{H_2,perm})^{0.5}]$ pressure difference. The permeability of H_2 was determined at different temperatures for the two membranes studied. The dependence of permeability with temperature was fitted with an Arrhenius type function:

$$Pe = Po \times e^{(-E/RT)} \quad (2)$$

where E is the apparent activation energy and Po, the pre-exponential factor (Po).

The values of both the activation energy and the pre-exponential factor obtained in this work (Table 3) are close to those reported in the literature for Pd membranes with several-micron thickness [20].The Pd/NaAPSS membrane has a higher permeability than the Pd–Ag membrane (Table 3). The ideal selectivity, defined as the ratio between the fluxes of the two pure gases (H_2 and N_2) under the same trans-membrane pressure difference and temperature, is included in Table 3. At 450-550 °C and a trans-membrane pressure of 50 kPa, no N_2 flux through the Pd–Ag commercial membrane was observed. This implied the absence of defects in the metal film or sealing leaks and assured 100% selectivity to hydrogen. In the case of the Pd/NaAPSS membrane, the ideal selectivity was close to 2000 and this value remained constant during hydrogen permeation measurements at 350–450 °C and a differential pressure of 100 kPa for 100 h. For this membrane, a linear increase of H_2 flow with the difference of the square root of the hydrogen partial pressure was also observed at different temperatures (not shown). In all cases, the linear regression gave an R-squared (R^2) value near 0.9998. This behavior suggests that the diffusion of hydrogen in the metallic film mainly obeys Sievert's law.

In a previous paper, we modeled the hydrogen transport properties of several Pd composite membranes and the solution-diffusion contribution could be isolated [9]. This allowed a more accurate estimation of Sieverts' transport parameters and a critical comparison with data reported in the literature. When the ideal selectivity was close to 1000, Sieverts' flux was higher than 99.6% of the total flow.

3.3. Catalytic behavior of $Ru/La_2O_2CO_3$ (Ru2MR) in the membrane reactors

3.3.1. Performance of the membrane reactor built with the composite Pd membrane at 450 °C.

Fig. 2a shows the methane conversion as a function of the sweep ratio for different feed conditions for the Ru2MR catalyst. Under DRM conditions, with increasing CO_2/CH_4 ratio, the CH_4 conversion increases 20%. However, when oxygen is added to the feed mixture, the CH_4 conversion shows a higher increase (conversion enhancement was 150%). For a sweep ratio over 8.7, the conversions of both CH_4 and CO_2 remain roughly constant except for the case of CRM with the CO_2/CH_4 ratio equal to 1.9. In this case, the CH_4 conversion increases with the sweep ratio (28% at SG ratio = 8.7–32% at 15.7).

Fig. 2b shows the H_2 permeated/CH_4 fed ratio as a function of the sweep gas ratio. The CRM curves are above those of DRM.

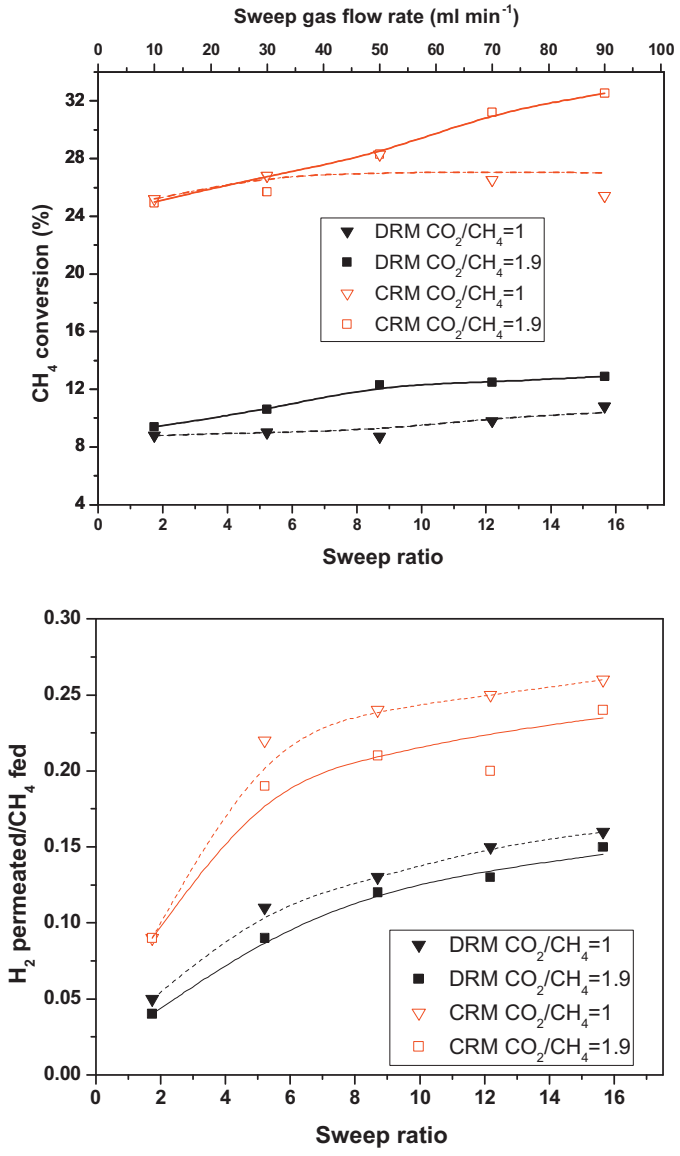

Fig. 2. CH_4 conversion (a) and H_2 permeated/CH_4 fed (b) as a function of sweep ratio (sweep gas flow/CH_4 fed). To vary the CO_2/CH_4 ratio the following CH_4:CO_2:Ar ratios were employed: [1:1:1.2] and [1:1.9:0.3] and with 10% of O_2 the CH_4:CO_2:O_2:Ar ratios were [1:1:0.3:0.9] and [1:1.9:0.3:0]. Pd composite membrane reactor, permeation area: 7.9 cm^2. T = 450 °C, ΔP = 0, W = 1.5 g, $W/F = 1.5 \times 10^{-3}$ g h ml^{-1}.

This means that the operating conditions of CRM not only yield a considerable increase in conversion but also result in an increased production of hydrogen. For CO_2/CH_4 ratios higher than the stoichiometric ratio (CO_2/CH_4 = 1.9), a slightly lower hydrogen flow was obtained.

The permeation selectivities (H_2/CH_4 ratio) observed during the DRM and CRM reactions are shown in Fig. 3. The H_2/CH_4 ratios increase with increasing sweep gas ratio (ΔP). Several factors could affect the hydrogen permeation when hydrogen is present in a gas mixture, such as the competitive adsorption of other gas components, which reduces the fraction of sites available for hydrogen adsorption and dissociation; the bulk gas depletion along the retentate side due to the selective removal of hydrogen, and the concentration polarization due to gas phase mass transport limitations [21].

This membrane was used in different atmospheres during 1000 h in a temperature range between 350 and 450 °C. The temperature was never over 450 °C.

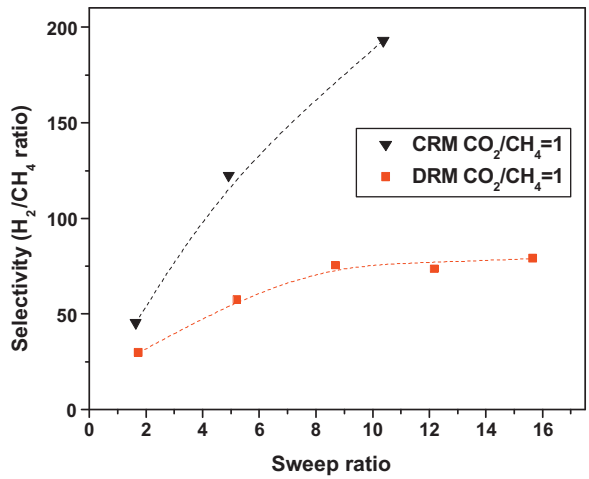

Fig. 3. Permeation selectivity (H_2/CH_4) as a function of sweep ratio under DRM and CRM conditions with a CO_2/CH_4 ratio = 1. Pd composite membrane reactor (Ru2MR), permeation area: 7.9 cm^2. T = 450 °C, ΔP = 0, W = 1.5 g, $W/F = 1.5 \times 10^{-3}$ g h ml^{-1}.

Oyama and Lim [22] performed the numerical simulation of a membrane reactor for the methane steam reforming and they found that membranes with H_2/CH_4 selectivities of 100 essentially showed the same enhancement of both the methane conversion and H_2 yield as the membrane with infinite hydrogen selectivity. This comparison was carried out at constant hydrogen permeance. They concluded that H_2/CH_4 permeation selectivities greater than 100 allowed a high yield in the MRs. The Pd/NaAPSS membrane selectivities were close to the values proposed by Oyama and Lim [22]. These values could explain the similar performance observed in both membrane reactors built with commercial and composite membranes.

Our palladium membrane exhibited the H_2/CH_4 selectivity in a range of 20–200 (Fig. 3), with a permeate hydrogen purity equal to 99.5%.

3.3.2. *Comparison of the two membranes at different temperatures*

Fig. 4a shows the methane conversions for both membranes under CRM conditions. The values of the thermodynamic equilibrium conversions at 450, 500 and 550 °C are also shown. They were calculated considering the simultaneous occurrence of the following reactions: dry reforming, reverse water gas shift, partial and total oxidation of methane.

The Pd/NaAPSS membrane reactor has the limitation that it could be operated only at temperatures as high as 450 °C, while the commercial reactor could also be operated at 500 and 550 °C. The conversion increased with the sweep gas ratio at 500 and 550 °C. At 450 °C, conversion was constant in both membrane reactors. The increase in CH_4 conversion for the Pd–Ag membrane was 15% with respect to the equilibrium values at 550 °C. In all cases, the carbon balance was higher than 98.5%, indicating that no coke deposition occurred.

The H_2 permeated/CH_4 fed ratio increases with the sweep gas ratio (Fig. 4b). Additionally, this ratio shows a significant increase with the reaction temperature, reaching a value of 0.55 at 500 °C and 0.82 at 550 °C when the maximum sweep gas ratio was employed for the Pd–Ag membrane. Note that the H_2 permeability increases with temperature when the permeation follows the solution-diffusion mechanism described by Sieverts' law (Table 3). The Pd membrane reactor exhibits a higher H_2 permeated/CH_4 fed ratio increase with the sweep gas ratio at 450 °C that could be related to its higher hydrogen permeability.

Another key parameter for membrane reactors is the hydrogen recovery defined as the ratio of the H_2 permeated and the total H_2

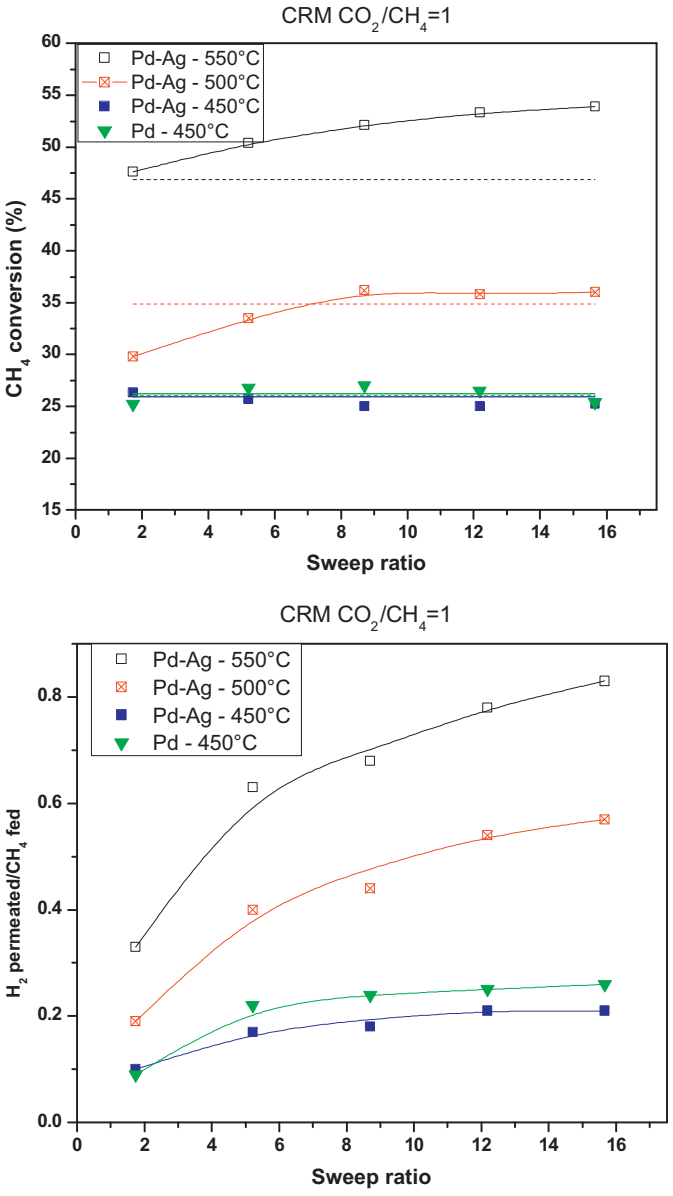

Fig. 4. CH_4 conversion (a) and H_2 permeated/CH_4 fed (b) as a function of sweep ratio under CRM conditions. Pd (▼) and Pd–Ag (■) membrane reactor, permeation area = 7.5 (Pd–Ag) and 7.9 cm^2 (Pd), T = 450–550 °C, $\Delta P = 0$, $W = 1.5$ g, $W/F = 1.5 \times 10^{-3}$ g h ml^{-1}.

produced. The recoveries of Pd and Pd–Ag membrane reactors as a function of the sweep gas ratio were studied (not shown). For CRM conditions with $CO_2/CH_4 = 1$ at 450 °C, the recovery values were similar for both membrane reactors. The H_2 recovery reached 72% for both membranes with different permeabilities and H_2/CH_4 selectivities.

The commercial membrane showed a value close to 80% hydrogen recovery at 550 °C when the sweep ratio was 16. In addition, the Pd composite membrane produced hydrogen with 99.5% of purity; this value was calculated considering only H_2 and the permeated gases.

3.3.3. *Effect of the CO_2/CH_4 ratio and the influence of the sweep gas ratio on hydrogen production with a commercial PdAg membrane reactor at 550 °C*

The effect of the CO_2/CH_4 ratio and the sweep gas ratio was also studied on the commercial membrane reactor at high temperature because of the maximum heating temperature allowed in the PdAg membrane (600 °C). Table 4 shows the influence of the sweep gas (SG) flow rate on the conversion of methane and carbon dioxide for DRM and CRM using a CO_2/CH_4 equal to 1 at 550 °C. When the SG flow rate increases, methane conversions exceed the equilibrium values. The CH_4 and CO_2 conversions reach similar values for DRM. Additionally, the H_2/CO ratio increases from 0.79 to 0.87. These results suggest that the hydrogen separation in the membrane reactor is unfavorable for the RWGS reaction when the reactor is operated at atmospheric pressure, consistent with that observed for $Ru/La_2O_3(50)–SiO_2$ [11]. It should be remarked that the conversions of both CH_4 and CO_2 remained constant above 30 ml min^{-1} with increasing the SG flow rate.

As mentioned above, when oxygen is added to the feed mixture (CRM), the reactions that might occur on the catalytic bed over the membrane are the partial oxidation of methane and the dry reforming reaction, in addition to the reverse or direct water gas shift reaction and total oxidation of methane. As a consequence of these reactions, the carbon dioxide conversion is significantly lower than the methane conversion and the H_2/CO ratio is much higher than 1. When the sweep gas flow rate increases, the retentate hydrogen partial pressure is always higher for the CRM reaction system compared with DRM conditions (Table 4). The same behavior is observed when this ratio is equal to 1.9 (not shown).

Fig. 5 shows the methane conversion as a function of the sweep ratio for different feed conditions for the Ru2MR catalyst at 550 °C. The catalytic behavior is similar to that observed at 450 °C, although the conversions are higher. Under DRM conditions, with increasing CO_2/CH_4 ratio, the CH_4 conversion increases only 10%. However, when oxygen is added to the feed mixture, the CH_4 conversion shows a larger increase. Under CRM conditions with increasing CO_2/CH_4 ratio, no increase in the CH_4 conversion is observed. For a sweep ratio over 8, the conversions of both CH_4 and CO_2 remain roughly constant.

For ethanol steam reforming, Gallucci et al. [16] reported that the highest increase in the ethanol conversion was observed in the sweep ratio 1–8 range. Afterwards, the conversion reached a plateau. They remarked that an increase of the sweep ratio just makes the hydrogen containing stream in the shell

Table 4
CH_4 and CO_2 conversions and H_2 produced/CO ratios for Ru2MR catalyst in DRM and CRM conditions on commercial membrane reactor.

SG [ml min^{-1}] (sweep ratio)	X_{CH_4}		X_{CO_2}		H_2/CO[b]		P_{H_2}[c]	
	DRM[a]	CRM[a]	DRM[a]	CRM[a]	DRM[a]	CRM[a]	DRM[a]	CRM[a]
10 (1.7)	31.0	47.6	32.1	12.6	0.79	1.32	12.12	15.85
30 (5.2)	36.2	50.4	39.2	15.2	0.85	1.45	9.20	10.50
50 (8.7)	37.7	52.1	36.9	13.2	0.84	1.45	7.68	8.23
70 (12.2)	36.0	53.3	39.8	11.4	0.86	1.56	6.47	6.95
90 (15.7)	37.4	53.9	40.0	12.4	0.87	1.55	5.42	6.07

[a] $CO_2/CH_4 = 1$, permeation area: 6 cm^2, catalyst mass = 1.5 g, $W/F = 1.5 \times 10^{-3}$ g h ml^{-1}, P = 101 kPa, T = 550 °C. CRM [CO_2:CH_4:O_2] = [1:1:0.3].
[b] Total hydrogen (retentate + permeated)/CO ratio.
[c] Retentate hydrogen partial pressure [kPa].

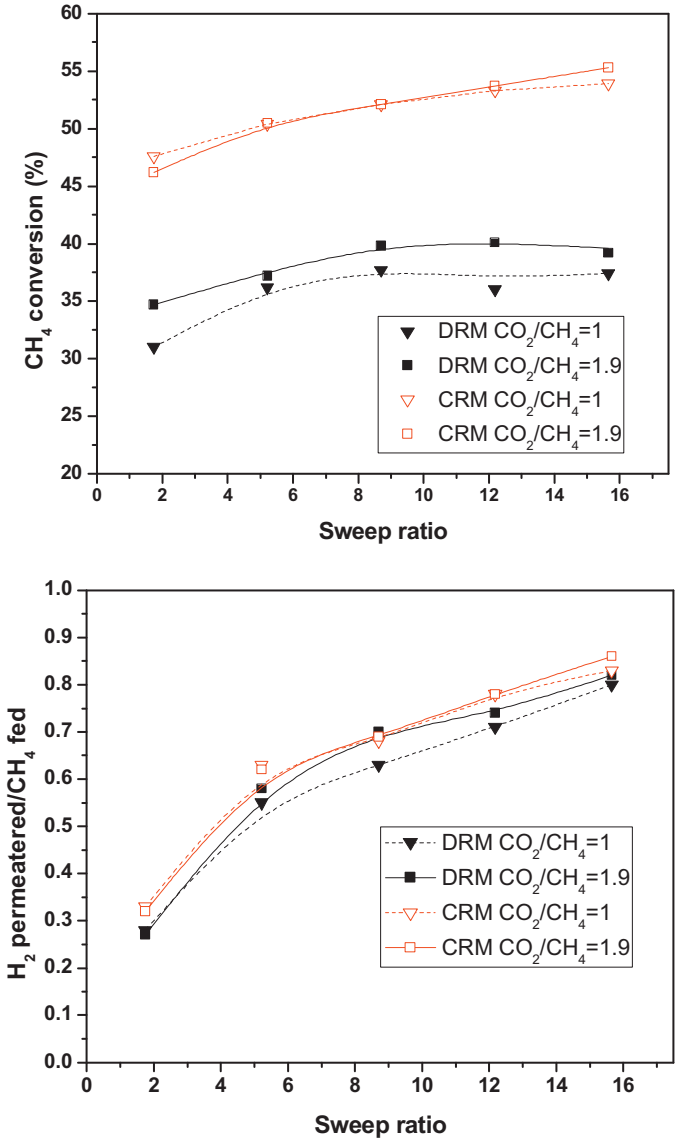

Fig. 5. CH_4 conversion (a) and H_2 permeated/CH_4 fed (b) as a function of sweep ratio for the different feed mixtures under DRM and CRM conditions. To vary the CO_2/CH_4 ratio, the following CH_4:CO_2:Ar ratios were employed: [1:1:1.2] and [1:1.9:0.3] and with 10% of O_2 the CH_4:CO_2:O_2:Ar ratios were [1:1:0.3:0.9] and [1:1.9:0.3:0]. Commercial membrane reactor with permeation area: 6 cm^2. T = 550 °C, ΔP = 0, W = 1.5 g, $W/F = 1.5 \times 10^{-3}$ g h ml^{-1}.

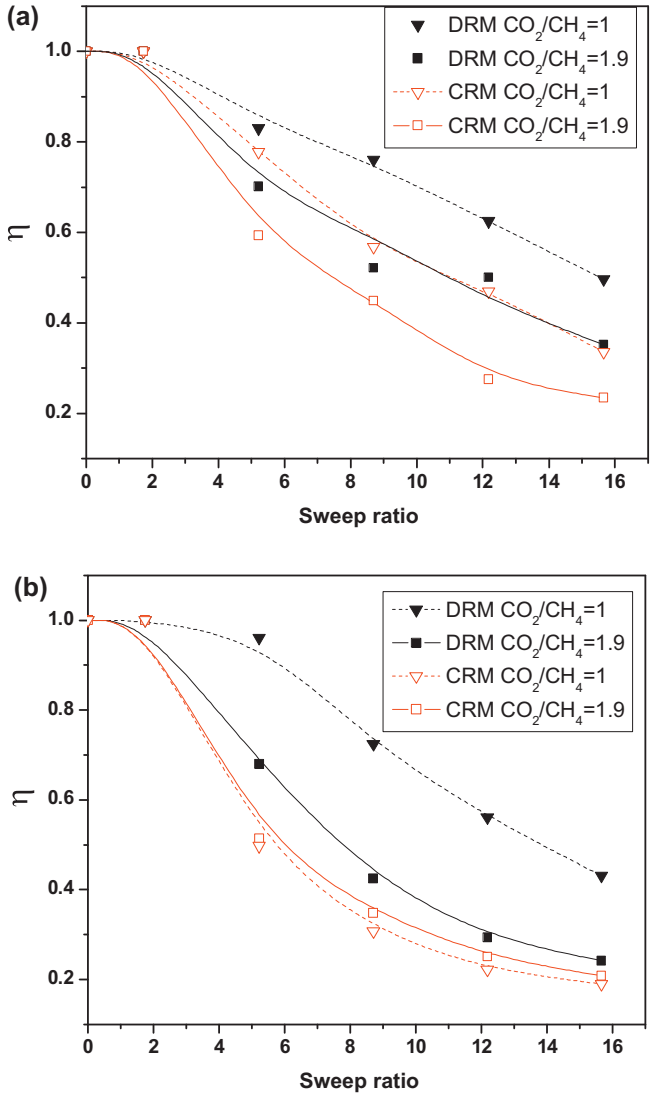

Fig. 6. Ability of the catalyst to keep the retentate equilibrated when the membrane reactor was built with a Pd–Ag commercial membrane (permeation area = 6 cm^2) as a function of sweep ratio: (a) for Ru/La_2O_3(50)–SiO_2 and (b) for Ru2MR. T = 550 °C, ΔP = 0, catalyst mass = 1.5 g, $W/F = 1.5 \times 10^{-3}$ g h ml^{-1}.

side much diluted without any benefit in terms of reactor performance.

Fig. 5b shows the H_2 permeated/CH_4 fed ratio as a function of the sweep gas ratio. The CRM curves are always slightly higher than those of DRM. This means that the operating conditions of CRM not only yield a considerable increase in conversion but also result in an increased production of hydrogen.

3.4. Comparison of both catalysts: Ru2MR vs Ru/La_2O_3–SiO_2

To describe the optimal operation of membrane reactors, different approaches have been reported in the literature [23–25]. Oyama and Lim [22] employed the ratio of product permeation and formation rates called operability level coefficient (OLC). Note that this ratio is in agreement with the commonly used hydrogen recovery or separation ratio. They found an interesting correlation between the OLC and hydrogen yield and conversion enhancements for steam and CO_2 reforming reactions. They also studied the relationship between membrane reactor performance measured by conversion or yield enhancements with membrane permeances [26]. We have applied the same correlation for the methane conversion enhancement as a function of hydrogen recovery, reaching enhancements of approximately 90% for recoveries close to 85% [9,27].

To take into account the catalyst activity and its ability to restore the chemical equilibrium upon H_2 withdrawal, an equilibrium fraction of the dry reforming reaction of methane can be defined, [10,24,25] as follows:

$$\eta = \frac{\prod_i p_i^{vi}}{K_{eq}} \quad (4)$$

where *pi* is the partial pressure of each reactant and product in the reaction side of the membrane reactor, *vi* are the DRM stoichiometric numbers, and K_{eq} is the equilibrium constant (evaluated in the fixed-bed reactor, which is close to the value calculated from free energy of formation). This fraction shows the approach to equilibrium of this reaction. If the composition

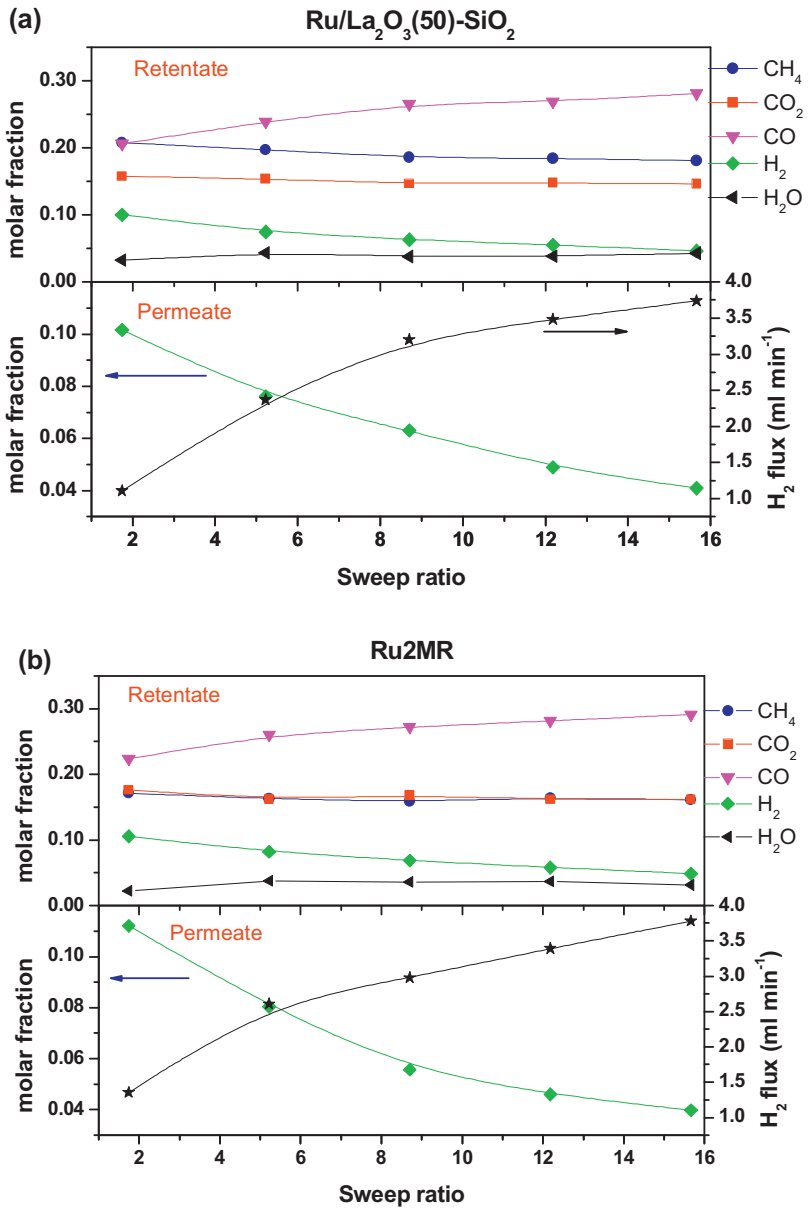

Fig. 7. Variation of the different species with the increase of the sweep ratio for DRM conditions with CO_2/CH_4 ratio = 1; (a) for $Ru/La_2O_3(50)–SiO_2$ and (b) for Ru2MR. $T = 550\,^{\circ}C$, $\Delta P = 0$, catalyst mass = 1.5 g, $W/F = 1.5 \times 10^{-3}$ g h ml^{-1}.

corresponds to thermodynamic equilibrium, this ratio is equal to 1.

In this work, we compared the catalytic behavior in a membrane reactor of Ru supported on either high surface area lanthanum oxycarbonate or $La_2O_3–SiO_2$ binary support. A complete study for the latter catalyst has been previously published [11,28]. The η values calculated for different feed conditions for both catalysts are shown in Fig. 6a and b.

For all the cases, η starts from unit and, when the sweep ratio is higher than 5.3, the η value decreases indicating that when high H_2 is removed from the system, the catalyst cannot restore the equilibrium. This behavior is less pronounced for Ru2MR or DRM conditions with a CO_2/CH_4 ratio equal to 1. In this case, η starts from unit and is maintained until a sweep ratio equal to 5.3. When this ratio is equal to 8.7, the η value decreases to 0.75, and for higher sweep ratios it continues to decline. In the case of the CRM reaction, the same behavior is observed but even more pronounced.

3.5. Gas compositions on both sides of the membrane

We studied the variation in the gas composition on both sides of the membrane for $Ru/La_2O_3(50)–SiO_2$ and Ru2MR, as a function of the sweep gas flow rate. The results for DRM with a CO_2/CH_4 ratio equal to 1 are shown in Fig. 7. The molar fraction of CO increases in the reaction side, whereas the molar fractions of CO_2, CH_4 and H_2 decrease. The molar fraction of H_2 in the permeate side decreases due to the dilution effect of the sweep gas. The membrane is 100% selective to hydrogen and this gas is only detected on the permeate side. The increased flow of Ar as sweep gas reduces the hydrogen partial pressure on the permeate side, which leads to a higher H_2 flow through the membrane.

The molar fractions of CO_2 and CH_4 are coinciding for the Ru2MR catalyst, suggesting that this solid does not favor the RWGS reaction (Fig. 7b). These results explain the higher H_2 permeated/CH_4 fed ratio observed for this solid, which presents a lower conversion in all flow conditions under study [11].

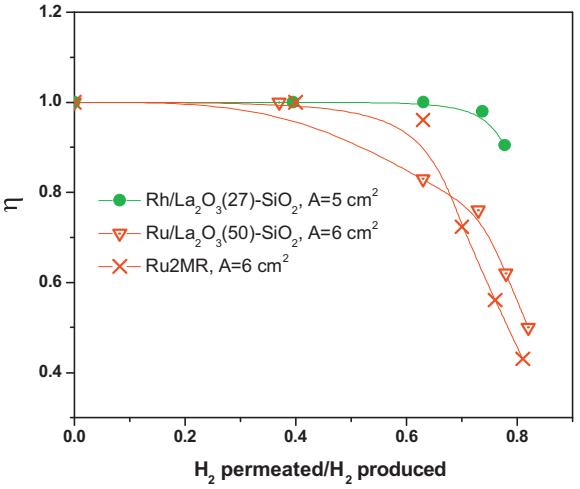

Fig. 8. Variation of the equilibration reaction ratio as a function of H_2 permeated/H_2 produced for the dry reforming reaction. Pd–Ag membrane reactor, Reaction temperature = 550 °C. A = permeation area, $W/F = 1.5 \times 10^{-3}$ g h ml^{-1}.

Note that after each catalytic test, we measured the permeability of the membrane. It did not show any variation in the hydrogen permeability and revealed no visual damage or carbon deposition. Furthermore, on the used catalysts carbon deposition was not detected by TGA measurements. However, a small quantity of graphitic carbon was detected by Laser Raman Spectroscopy because this technique is much more sensitive.

3.6. Comparison of Rh and Ru catalysts supported on lanthanum based substrates evaluated in membrane reactors

The fraction of the reaction equilibration (η) and the H_2 permeated/(CH_4 fed × permeation area) ratio were employed to compare the performance of Rh and Ru catalysts in membrane reactors. The membrane reactor applied was built with a commercial PdAg membrane with a permeance of 5.7×10^{-5} mol s^{-1} m^{-2} Pa$^{-0.5}$. The best catalysts developed in our group were selected for this comparison, Rh and Ru supported on La_2O_3–SiO_2 and Ru/$La_2O_2CO_3$ (Ru2MR).

For the dry reforming of methane reaction with $CO_2/CH_4 = 1$, the following order of activity was found for these catalysts: Rh/La_2O_3–SiO_2 > Ru/La_2O_3–SiO_2 > Ru2MR [5,11,19]. An increase in methane conversion was observed in the membrane reactor when compared with the conventional fixed bed reactor for all catalysts. Fig. 8 shows the η values determined for DRM at 550 °C. When a high hydrogen recovery was reached (close to 80%), the Rh solid could keep a η value equal to 0.9. This would indicate that for the most active catalyst, it would be possible to obtain a high hydrogen recovery maintaining the capacity to restore the thermodynamic equilibrium. This behavior could be related to the high activity of this La_2O_3–SiO_2 solid [5]. On the other hand, the Ru/La_2O_3(50)–SiO_2 and Ru2MR solids show a similar behavior; the reaction equilibration ratio begins to diminish when the hydrogen recovery is higher than 60%.

To perform a better comparison between catalysts, the H_2 permeated/CH_4 fed ratio was re-calculated taking into account the permeation flux expressed by permeation area (mol s^{-1} m^{-2}). These values are shown in Fig. 9a and b for DRM and CRM conditions, in both cases a reactant ratio equal to 1 was employed. In the case of CRM conditions, all catalysts show the same performance; however, the Ru2MR and the Rh solids exhibit ratios higher than those observed for Ru/La_2O_3(50)–SiO_2 when the dry reforming of

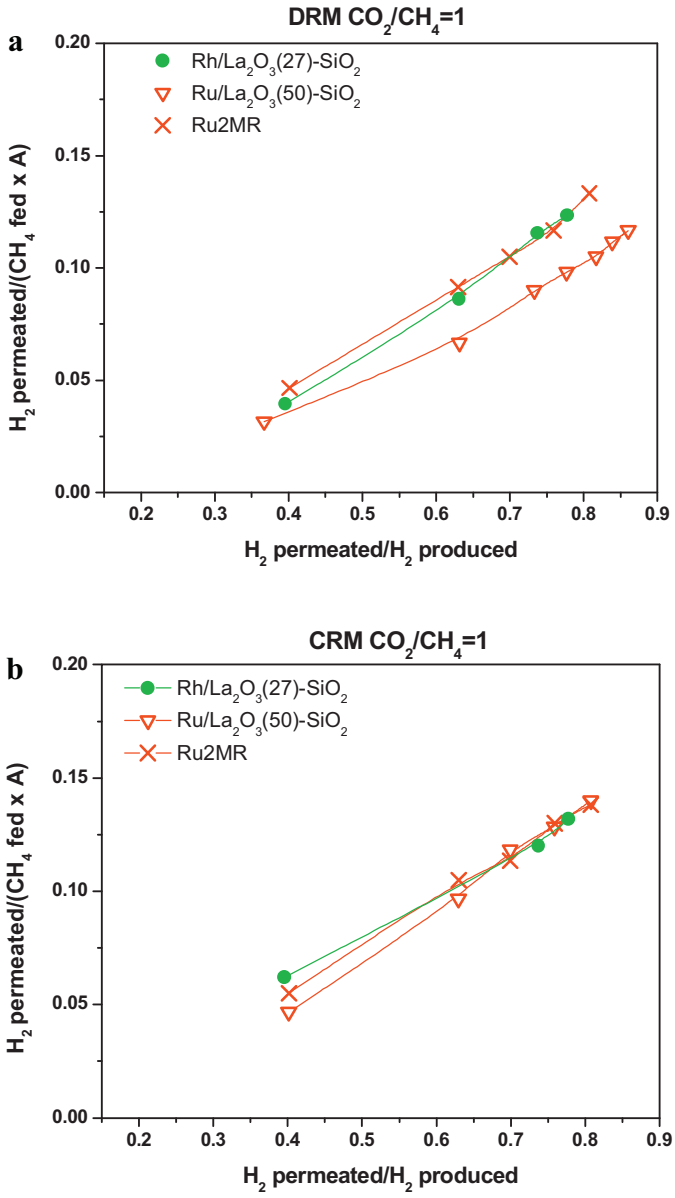

Fig. 9. H_2 permeated/(CH_4 fed × permeation area) as a function of H_2 permeated/H_2 produced for the dry reforming (a) and combined reforming of methane reaction (b). Pd–Ag membrane reactor, reaction temperature = 550 °C. A = permeation area, $W/F = 1.5 \times 10^{-3}$ g h ml^{-1}.

methane was carried out. The high ratio of Ru2MR compared with Ru supported on the binary substrate is in agreement with the gas composition results in which it could be observed that the RWGS reaction is not favored.

4. Conclusions

Ruthenium catalysts supported on lanthanum oxycarbonate ($La_2O_2CO_3$) with high surface area were stable for at least 90 h on stream. The Ru2MR catalyst was selected for study in the membrane reactors because the metallic Ru species were more stable even at increasing severity.

The double tubular membrane reactor was built using a commercial self-standing membrane or a composite Pd/NaAPSS membrane. The latter could be operated at temperatures as high as 450 °C, while the commercial reactor was also operated at 500

and 550 °C for DRM and CRM. The Pd membrane reactor exhibited a higher H_2 permeated/CH_4 fed ratio increase with the sweep gas ratio at 450 °C that could be related to its higher hydrogen permeability.

The H_2 permeated/CH_4 fed ratio values for CRM conditions were slightly higher than those of DRM. This means that the operating conditions of CRM not only yield a considerable increase in conversion but also result in an increased production of hydrogen.

The molar fractions of CO_2 and CH_4 are similar for the Ru2MR catalyst, suggesting that this solid does not favor the RWGS reaction for DRM conditions. These results explain the higher H_2 permeated/CH_4 fed ratio observed for this solid, which presents a lower conversion in all the explored flow conditions compared with the $Ru/La_2O_3(50)–SiO_2$ catalyst previously studied.

The Ru catalysts show a high potential for application in membrane reactors because they exhibit a similar performance to Rh solids with a ten-time lower cost (Rh price per gram/Ru price per gram = 7–10).

Nomenclature

W	catalyst weight [g]
F	total flow rate [ml h^{-1}]
o.d.	outside diameter [mm]
i.d.	inside diameter [mm]
Pe	permeability [mol s^{-1} m^{-2} $Pa^{-0.5}$]
K	permeance [mol s^{-1} m^{-1} $Pa^{-0.5}$]
J	permeation flux [mol s^{-1}]
n	value of exponent of the permeate and retentate pressures
$P_{H2,ret}$	hydrogen pressure in retentate side [Pa]
$P_{H2,perm}$	hydrogen pressure in permeate side [Pa]
l	membrane thickness [m]
E	apparent activation energy [kJ mol^{-1}]
Po	pre-exponential factor [mol m^{-1} s^{-1} $Pa^{-0.5}$]
R	ideal gas constant [kJ mol^{-1} K^{-1}]
T	temperature [K]
η	equilibrium fraction of the dry reforming reaction of methane
pi	partial pressure of each reactants and products in the reaction side of the membrane reactor [atm]
νi	DRM stoichiometric numbers
K_{eq}	equilibrium constant

Acknowledgements

The authors wish to acknowledge the financial support received from UNL, ANPCyT and CONICET. Thanks are also to Elsa Grimaldi for the English language editing.

References

[1] D. Lee, P. Hacarlioglu, S.T. Oyama, Topics in Catalysis 29 (2004) 45–57.
[2] P. Ferreira-Aparicio, M. Benito, S. Menad, Journal of Catalysis 231 (2005) 331–343.
[3] S.T. Oyama, P. Hacarlioglu, Y. Gu, D. Lee, International Journal of Hydrogen Energy 37 (2012) 10444–10450.
[4] H. Chang, W. Pai, Y. Chen, W. Lin, International Journal of Hydrogen Energy 35 (2010) 12986–12992.
[5] J.F. Múnera, C. Carrara, L.M. Cornaglia, E.A. Lombardo, Chemical Engineering Journal 161 (2010) 204–211.
[6] M.E. Ayturk, E.E. Engwall, Y.H. Ma, Industrial and Engineering Chemistry Research 46 (2007) 4295–4302.
[7] C. Su, T. Jin, K. Kuraoka, Y. Matsumura, T. Yazawa, Industrial and Engineering Chemistry Research 44 (2005) 3053–3061.
[8] M.L. Bosko, F. Ojeda, E.A. Lombardo, L.M. Cornaglia, Journal of Membrane Science 331 (2009) 57–65.
[9] M.L. Bosko, J.F. Múnera, E.A. Lombardo, L.M. Cornaglia, Journal of Membrane Science 364 (2010) 17–26.
[10] J.F. Múnera, L. Coronel, B. Faroldi, C. Carrara, E.A. Lombardo, L.M. Cornaglia, Asia-Pacific Journal of Chemical Engineering 5 (2010) 35–47.
[11] B.M. Faroldi, E.A. Lombardo, L.M. Cornaglia, Catalysis Today 172 (2011) 209–217.
[12] B. Faroldi, C. Carrara, E.A. Lombardo, L. Cornaglia, Applied Catalysis A: General 319 (2007) 38–46.
[13] R. Cantrell, A. Ghenciu, K. Campbell, A. Minahan, M. Bhasin, A. Westwood, K. Nielsen, US Patent 2002/0173420 (2002), p. A1.
[14] F. Guazzone, E.E. Engwall, Y.H. Ma, Catalysis Today 118 (2006) 24–31.
[15] P.P. Mardilovich, Y. She, Y.H. Ma, M. Rei, AIChE Journal 44 (1998) 310–322.
[16] F. Gallucci, M. De Falco, S. Tosti, L. Marrelli, A. Basile, International Journal of Hydrogen Energy 33 (2008) 644–651.
[17] C. Carrara, J. Múnera, E. Lombardo, L. Cornaglia, Topics in Catalysis 51 (2008) 98–106.
[18] N. Matsui, K. Anzai, N. Akamatsu, K. Nakagawa, N. Ikenaga, T. Suzuki, Applied Catalysis A: General 179 (1999) 247–256.
[19] B. Faroldi, J. Múnera, L. Cornaglia, Applied Catalysis B: Environmental, submitted for publication.
[20] M.L. Bosko, E.A. Lombardo, L.M. Cornaglia, International Journal of Hydrogen Energy 36 (2011) 4068–4078.
[21] L. Mejdell, M. Jondahl, T.A. Peters, R. Bredesen, H.J. Venvik, Journal of Membrane Science 327 (2009) 6–10.
[22] S.T. Oyama, H. Lim, Chemical Engineering Journal 151 (2009) 351–358.
[23] C. Reo, L. Bernstein, C. Lund, Chemical Engineering Science 52 (1997) 3075–3083.
[24] L. Li, R.W. Borry, E. Iglesia, Chemical Engineering Science 57 (2002) 4595–4604.
[25] D. Ma, C.R.F. Lund, Industrial and Engineering Chemistry Research 42 (2003) 711–717.
[26] H. Lim, Y. Gu, S.T. Oyama, Journal of Membrane Science 396 (2012) 119–127.
[27] L. Coronel, J.F. Múnera, E.A. Lombardo, L.M. Cornaglia, Applied Catalysis A: General 400 (2011) 185–194.
[28] B.M. Faroldi, E.A. Lombardo, L.M. Cornaglia, Applied Catalysis A: General 369 (2009) 15–26.